Quantum migration and its local heat impact: Understanding local heat capacity of confined systems

Altug Sisman [*] and Jonas Fransson [†]
Department of Physics and Astronomy, Uppsala University, Box 516, 751 21 Uppsala, Sweden

(Received 20 October 2023; revised 16 April 2024; accepted 19 August 2024; published 5 September 2024)

For noninteracting particles confined in a constant volume, the temperature derivative of the local energy assumes negative values in thermodynamic equilibrium at low temperatures. This peculiar behavior may entail the misleading unphysical conclusion that the local heat capacity is negative. However, we show that temperature-dependent density variations of confined particles induce an energy selective particle transport within the domain, here called *temperature-induced quantum migration*. This macroscopic quantum phenomenon causes a redistribution of local heat and ensures a non-negative local heat capacity. Moreover, it induces local heating and cooling effects and a massive overshoot in local heat capacity. The quantum migration also builds up the thermal part of confinement energy, manifesting in an excess global heat capacity. Analyzing the local energy fluctuations shows that the linear relationship between heat capacity and fluctuations is broken at the local scale.

DOI: 10.1103/PhysRevE.110.034112

I. INTRODUCTION

Confinement effects on material behaviors have been extensively studied in the past few decades, holding the promise for developments of superior materials [1]. Quantum size and shape effects on thermodynamic properties are some of the main topics in this direction [2–33]. At the nanoscale, size and shape become control parameters on thermodynamic state functions and open up new possibilities to further enhance the materials and design entirely novel energy conversion devices [24,27–29,34–36]. In the thermodynamics of confined systems, global properties are usually the focus, which are calculated directly from their fundamental definitions based on, e.g., infinite summations over the discrete energy eigenvalues.

The heat capacity of noninteracting particles in a finite box is a long-standing open problem that was launched already in the 1960s and has been repeatedly considered ever since [2,37–41]. Specifically, the properties of nanoscale heat capacity have been extensively studied [2,3,31,32,37–47], holding a promise of an adjustable excess heat capacity for nanoscale materials. In the case of Maxwell-Boltzmann statistics, for each confined direction, the heat capacity per particle reaches an excess value of $9/16 \simeq 0.56$ for a specific temperature or size, compared to the corresponding classical value $1/2$. The excess heat capacity originates from the thermal part of confinement energy which, in turn, is induced by quantum size effects [2–13,15,20,22,31].

For a fixed size system, heat capacity is a measure of the temperature variations of, e.g., the energy. The energy, in turn, depends not only on temperature but also on the density and its distribution, which is inhomogeneous and controlled by temperature, even in noninteracting confined systems [14,16,17]. However, while the temperature dependence of the density distribution is crucial in local heat capacity problems, it has hitherto been completely overlooked in finite systems.

Hence, in this study, we consider noninteracting particles in a domain of fixed size and investigate the *local* heat capacity in equilibrium. We show that the temperature derivative of the local energy, $\partial u/\partial T$, assumes negative values around the center of the box at low temperatures. Despite this local negativity, the *global* heat capacity, which is the domain integral of $\partial u/\partial T$, is positively definite. Conceptually, a negative value for the temperature derivative of the local energy is deceptive since it may be associated with a negative local heat capacity. This is especially compelling in the light of the existence of negative global heat capacity, which has been demonstrated for interacting particles under equilibrium or nonequilibrium conditions, in, e.g., nanoclusters, self-gravitating bodies, and some structures with nonuniform confinement potential specifically designed for the purpose [42–51]. However, for noninteracting particles in equilibrium, coexistence of negative and positive local heat capacity regions leads to instabilities which contradict the equilibrium condition and is, hence, unphysical. Therefore, for nanoscale systems, the local heat capacity cannot be equal to the temperature derivative of the local energy. Here, we resolve this issue by introducing the concept of *temperature-induced quantum migration* of particles and its heat impact in nanoscale systems, which ensures that the local heat capacity is non-negative. Furthermore, we demonstrate that local heat capacity exhibits a significant overshoot, which has both academic and practical implications for researchers seeking to develop theoretical models and technological devices.

Confinement changes the energy levels of particles and hence the associated properties of nanoscale materials. The change in energy levels leads to the formation of confinement energy, which plays a significant role in the unusual and

[*]Contact author: altug.sisman@physics.uu.se
[†]Contact author: jonas.fransson@physics.uu.se

Published by the American Physical Society under the terms of the Creative Commons Attribution 4.0 International license. Further distribution of this work must maintain attribution to the author(s) and the published article's title, journal citation, and DOI. Funded by Bibsam.

superior behaviors exhibited by nanoscale materials. These exceptional behaviors cover a wide range of properties, including thermal, electrical, optical, magnetic, and mechanical properties. Excess heat capacity, enhanced thermoelectric properties, reduced thermal conductivity, increased band gap, discrete conductance, and tunable emissions are just some of them. Therefore, confinement energy leads to the development of advanced technologies, such as high-capacity thermal energy storage, high-efficiency thermoelectric devices, and others. Here, we show that the thermal component of confinement energy is built up by the quantum migration process, a macroscopic quantum phenomenon. In the conclusion section, we also discuss a possible experimental verification of temperature-induced quantum migration and a massive local heat capacity as a macroscopic quantum phenomenon.

II. LOCAL HEAT CAPACITY AT NANOSCALE

For a closed *simple* system of fixed size, the total heat exchange equals the internal energy change, since the thermodynamic work is zero. Therefore, the heat capacity at constant size, C_L, is given by

$$C_L = \left(\frac{\delta Q}{dT}\right)_L = T\left(\frac{\partial S}{\partial T}\right)_L = \left(\frac{\partial U}{\partial T}\right)_L. \tag{1}$$

Here, L represents the generalized set of size variables including not only volume but also the lower dimensional geometric variables (i.e., surface area, periphery, and number of corners or vertices), δQ is the exchanged heat, T is the temperature, U is the internal energy, and S is the entropy. The lower dimensional geometric measures are the geometric variables of Weyl's conjecture, which describes the asymptotic behavior of the number of eigenvalues of the Laplace Beltrami operator [52,53]. As a result of Weyl's conjecture, the number of states and the density of states functions depend not only on volume but also on surface area, periphery, and number of corners and vertices of the domain in general [20]. Therefore, all thermodynamic state functions become dependent on the geometric variables of Weyl's conjecture in general [5–14,16,17,27,28]. Although these dependencies are negligible for macroscopic systems, they become significant at the nanoscale. Consequently, any variation in these lower-dimensional geometric parameters induces work exchange at the nanoscale, even when the overall volume remains unchanged. Thus, in systems where at least one size is at the nanoscale, the traditional constant volume condition is insufficient to ensure zero work exchange. Instead, an *isometric condition* (constant size) must be applied. In this study, we examine such a finite system to rigorously analyze the local heat capacity and establish a precise definition tailored to nanoscale constraints.

In an isometric and macroscopic closed system comprising N noninteracting particles, the probability to find a particle in a specific location is constant, given by the reciprocal of the confinement volume $1/V$. Therefore, the local density n is equal to the average or global density, $n_{Gl} = N/V$. Due to the constant uniformity of density, the net particle transport within the system during heat exchange processes is zero. In other words, for an isometric process, local thermodynamic quantities are governed by the closed system balance equations and they are directly proportional to the global ones through the classical probability density, $1/V$. In this sense, the local heat capacity of a macroscopic system is $c_L = C_L/V$. Henceforth, the uppercase and lowercase letters refer to global and local quantities, respectively.

By contrast, in the quantum regime, the probability density is represented by the square modulus of the particle's wave function. In general then, the local density varies as a function of position and temperature, besides the size parameters [14,16,17,27]. As the particles in excited states have shorter wavelengths, they are more likely to occupy the boundary regions in comparison to the particles in the ground state or low-lying states, which have longer wavelengths and a tendency to concentrate within the central region of the confinement domain. Therefore, a change in temperature modifies the occupation numbers, which in turn changes the de Broglie wavelengths of the particles and results in a particle migration process from one local position to another. This migration is an energy-selective transport process, whereby only particles that undergo a transition from a low to a high energy state migrate from the central to the boundary regions. Conversely, an inverse transition results in a migration in the opposite direction. The energy-selective nature of this type of particle transport makes it distinct from the convection and advection, which are bulk motions of particles. Hence temperature variation induces changes in local density and gives rise to net flows of particles and energy from one region to another within the domain. These net flows of particle and energy are purely quantum phenomena emerging in nanoscale systems. Henceforth, this migration is referred to as *temperature-induced quantum migration (TIQM)*.

Because of the quantum migration process, a local differential control volume becomes an open subsystem of the globally closed system. Thus the local conductive heat exchange, δq^{cnd}, is not equal to $T\,ds$ but it is

$$\delta q^{\mathrm{cnd}} = Tnd\left(\frac{s}{n}\right) = T\,ds - T\left(\frac{s}{n}\right)dn, \tag{2a}$$

where the second term on the right hand side represents the quantum migration correction.

It should be noted that the heat transfer process under consideration is a quasistatic process, allowing the system to remain in both global and local equilibrium. In other words, the temperature difference is infinitesimally small, provided the temperature and chemical potential within the system are uniform. Furthermore, in Sec. IV, energy fluctuations in equilibrium at the global and local scales are analyzed in order to justify the results.

For the sake of completeness of the derivations and ease of calculation, we use not only the entropy representation but also the energy representation for the heat exchange process. Hence, using the fundamental laws of thermodynamics and considering zero work exchange through the external boundaries of the system, Eq. (2) can also be written as

$$\delta q^{\mathrm{cnd}} = du - \left[\mu + T\left(\frac{s}{n}\right)\right]dn = du - \left(\frac{\omega}{n}\right)dn, \tag{2b}$$

where u is the local energy, s/n is the local entropy per particle, μ is the chemical potential, $\omega = u - \varphi = \mu n + Ts$, and $\varphi = u - Ts - \mu n$ is the local grand potential.

Here, the relationship between the local pressure p and φ should be noted. The local pressure is defined as $p = -\{[\partial(f/n)/\partial v]\}_{T,L}$, where $f = u - Ts$ is the local free energy and $v = 1/n$ is the local volume per particle. For homogeneous systems, p and φ are simply related by $p = -\varphi$. A similar relation, $P = -(\Phi/V)$, also exists between the global pressure $P = -(\partial F/\partial V)_{T,N}$ and the global grand potential $\Phi = F - \mu N$ with free energy $F = U - TS$. At the nanoscale, however, quantum size effects appear and the homogeneity is broken. While the global pressure P becomes a vector quantity, the local pressure still remains as a scalar by its definition [9]. Also both global and local grand potentials remain scalar and unaffected from the size effects. Therefore, at nanoscale, the simple local relationship is preserved, $\varphi = -p$, while the global one is broken, $P \neq -(\Phi/V)$. Hence $\omega/n = (u + p)/n = h/n$ and the conductive heat is determined by subtraction of the enthalpy transport $(h/n)dn$ from the total internal energy change du, Eq. (2b). This is in agreement with the general balance equations for open systems [54]. Not subtracting the quantum migration terms in Eqs. (2a) and (2b) leads to unphysical results, including that of negative local heat capacity for noninteracting systems.

Due to the inhomogeneity, the local entropy per particle becomes position dependent, differing from the global average. As a result, when particles are transported isothermally between the local volume and the rest of the system, their entropy values change. This isothermal entropy change induces local heat exchange, akin to the Peltier effect [9,55]. Traditionally, the Peltier effect arises when an electric current passes through the isothermal junction of two dissimilar materials with different per-particle entropy values, leading to a sudden entropy change at the junction. In contrast, the heat effect discussed here emerges within a single material, not due to an electrical current driven by an external potential, but rather from quantum migration driven by a temperature change. This distinct local heat effect, resulting from quantum migration and the disparity in local entropy across the material, is termed *quantum migration heat (QMH)*. Consequently, the QMH also contributes to the local heat transfer. As we are considering an infinitesimal change of state during an infinitely slow heat exchange process, the QMH is proportional to the change in the number of particles in the local volume, dn, from an initial to a final state, $n \to n + dn$. Therefore, it is given by

$$\delta q^{\mathrm{qmh}} = T\left(\frac{s}{n} - \frac{S}{N}\right)dn. \tag{3a}$$

Considering the uniformity of chemical potential and temperature, Eq. (4) can also be expressed as

$$\delta q^{\mathrm{qmh}} = \left(\frac{\omega}{n} - \frac{\Omega}{N}\right)dn, \tag{3b}$$

where $\Omega = U - \Phi$. Consequently, at the nanoscale, the local heat exchange δq^{tot} comprises both conductive (cnd) and quantum migration heat (qmh) contributions, $\delta q^{\mathrm{tot}} = \delta q^{\mathrm{cnd}} + \delta q^{\mathrm{qmh}}$. Similarly, the local heat capacity c_L^{tot} can be defined as a summation of the contributions from both conductive heat and QMH, $c_L^{\mathrm{tot}} = c_L^{\mathrm{cnd}} + c_L^{\mathrm{qmh}}$. Below, we discuss those contributions separately in detail.

Using Eq. (2a), the conductive contribution to the local heat capacity in the entropy representation is determined as

$$c_L^{\mathrm{cnd}} = \left(\frac{\delta q^{\mathrm{cnd}}}{\partial T}\right)_L = c_L^{s,0} + \left(\frac{s}{n}\right)\gamma_L, \tag{4a}$$

where $c_L^{s,0} = T(\partial s/\partial T)_L$ is the entropy based local heat capacity without migration correction and $\gamma_L = -T(\partial n/\partial T)_L$ is the isometric thermal expansion coefficient of density. Note that there is no way to control the local density n to keep it constant as the temperature changes and applying a special temperature-controlled confinement potential is not a viable option as it would change the original system. Therefore, the total number of particles N and the global sizes of the domain L are the only parameters that we can keep constant throughout the derivations and the definitions of both local and global heat capacities.

In the energy representation, c_L^{cnd} is also expressed by using Eq. (2b) as

$$c_L^{\mathrm{cnd}} = c_L^{u,0} + \left(\frac{\omega}{nT}\right)\gamma_L, \tag{4b}$$

where $c_L^{u,0} = (\partial u/\partial T)_L$ is the energy based local heat capacity without migration correction. Notice that $c_L^{s,0} \neq c_L^{u,0}$ and they do not represent the true local heat capacity as the density depends on temperature. Similarly, considering Eq. (4b), $\int c_L^{\mathrm{cnd}}\, dV \neq C_L = \int c_L^{u,0}\, dV$ since $\int(\omega/n)\gamma_L dV \neq 0$ due to the position dependencies of ω/n, although $\int \gamma_L dV = 0$ as the total number of particles is conserved. The same holds true for Eq. (4a).

Similarly, using Eqs. (3a) and (3b), the QMH contributions to the local heat capacity in the entropy and energy representations are obtained respectively as

$$c_L^{\mathrm{qmh}} = \left(\frac{S}{N} - \frac{s}{n}\right)\gamma_L \tag{5a}$$

and

$$c_L^{\mathrm{qmh}} = \frac{1}{T}\left(\frac{\Omega}{N} - \frac{\omega}{n}\right)\gamma_L. \tag{5b}$$

Through the definitions of the conductive and quantum migration heat capacities, Eqs. (4a)–(5b), the local heat capacity can be determined by

$$c_L^{\mathrm{tot}} = c_L^{s,0} + c_L^{\mathrm{s,QC}} = c_L^{u,0} + c_L^{\mathrm{u,QC}}, \tag{6}$$

where $c_L^{\mathrm{s,QC}}$ and $c_L^{\mathrm{u,QC}}$ are the quantum corrections due to TIQM for $c_L^{s,0}$ and $c_L^{u,0}$ and they are defined as

$$c_L^{\mathrm{s,QC}} = \left(\frac{S}{N}\right)\gamma_L \tag{7a}$$

and

$$c_L^{\mathrm{u,QC}} = \frac{1}{T}\left(\frac{\Omega}{N}\right)\gamma_L. \tag{7b}$$

Notice that the domain integrals of $c_L^{\mathrm{s,QC}}$ and $c_L^{\mathrm{u,QC}}$ vanish since S and Ω have no spatial dependence and $\int \gamma_L dV = 0$.

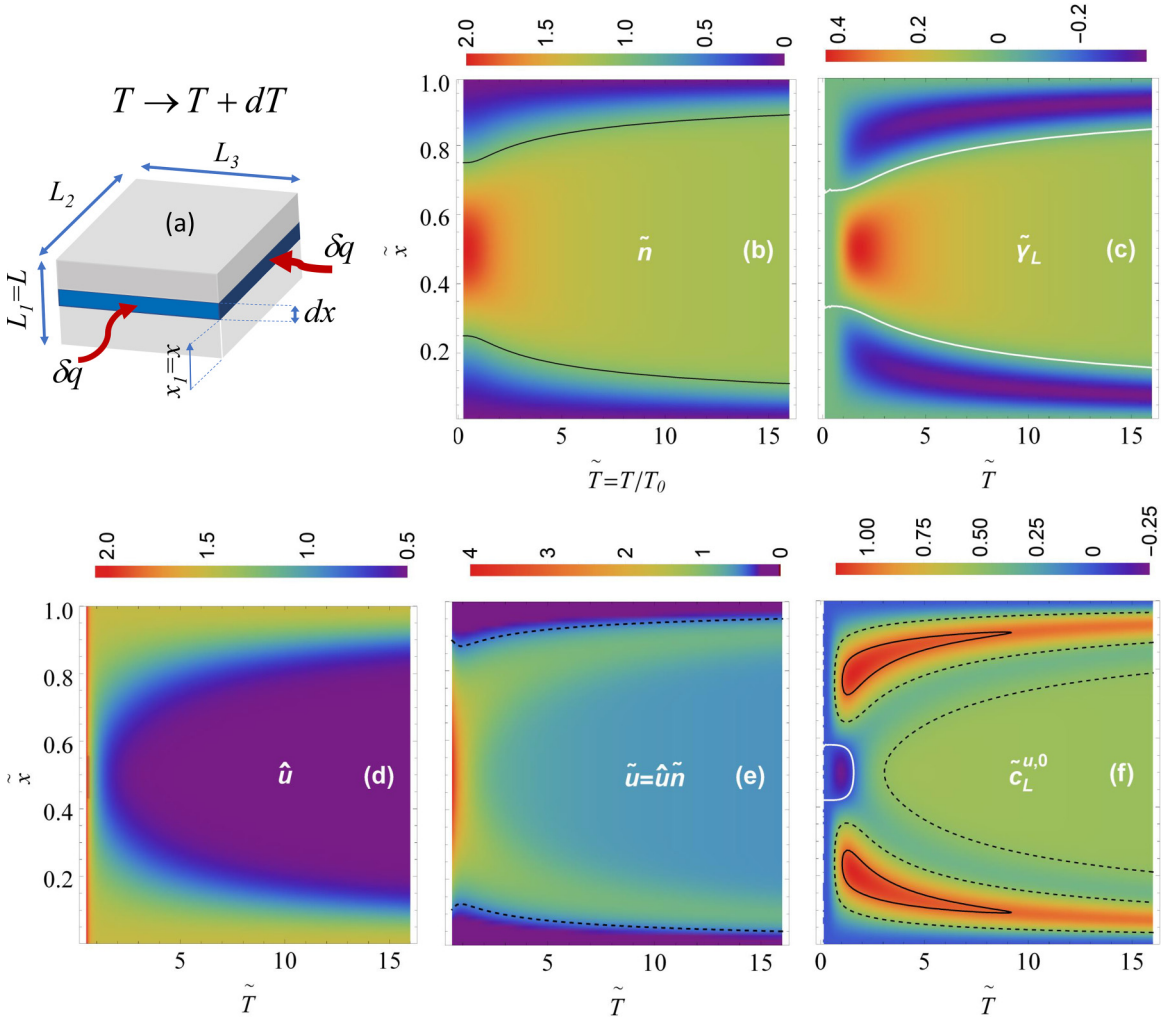

FIG. 1. Considered confinement domain and the local control volume highlighted by blue color at the middle (a), variations of density (b), isometric thermal expansion coefficient (c), local energy per particle (d), local energy (e), and the temperature derivative of local energy (f), with position $\tilde{x}$ and temperature $\tilde{T}$. Black and white curves represent the values of 1 and 0, respectively, while the dotted black ones in (e) and (f) stand for $1/2$.

Thus the uniformities of S and Ω guarantee that c_L^{tot} integrates to the global heat capacity. Although the entropy and energy representations of local heat capacity are equivalent as seen in Eq. (6), $c_L^{\text{s,QC}}$ and $c_L^{\text{u,QC}}$ are not equal each other, just like $c_L^{u,0} \neq c_L^{s,0}$.

In the macroscopic limit, the probability density approaches its classical value, $1/V$, such that the density tends to its global value, $n \to n_{Gl}$, which ensures that the quantum terms γ_L, $c_L^{\text{u,QC}}$, $c_L^{\text{s,QC}}$, and c_L^{qmh} all vanish and the classical result is recovered, i.e., $c_L^{\text{tot}} \to c_L^{\text{cnd}} \to c_L = C_L/V$. At the nanoscale, however, the introduced quantum migration is the key process for the correct definition of the local heat capacity, as we shall see in the following application.

III. APPLICATION FOR NONINTERACTING MAXWELL-BOLTZMANN GAS

While the results presented in Eqs. (1)–(7b) are generally valid, regardless of statistics and confinement geometry, we analyze and benchmark our theory with previous results [2,30,31,37]. For the sake of concreteness, we consider a dilute gas of noninteracting particles, hence, obeying Maxwell-Boltzmann statistics, which, for simplicity, are confined in a constant-size rectangular domain. The domain is confined in the first direction $\lambda_{\text{th}} \simeq \{0.25L_1 \ldots, 2.5L_1\}$, where $\lambda_{\text{th}} = 2\pi\hbar/\sqrt{2\pi m k_B T}$ is the thermal de Broglie wavelength with the particle mass m, Boltzmann's constant k_B, and the reduced Planck's constant $\hbar$, while it is practically free in the second and third directions, $\{L_2, L_3\} \gg \lambda_{\text{th}}$; see Fig. 1(a) for a schematic overview. Note that during the calculations, only the temperature, accordingly λ_{th}, is changed but the domain sizes, $\{L_1, L_2, L_3\}$, are kept constant.

MB statistics can only be used if the number of particles in the ground state is much smaller than one. This condition is met if λ_{th} is much shorter than the average interparticle distance calculated for at least one of the directions (sizes) of the domain. For the domain in Fig. 1(a), the condition is $\lambda_{th} \ll \sqrt{(L_2L_3)/N}$, which is satisfied even at low temperatures as long as L_2 and L_3 are long enough.

In Maxwell-Boltzmann statistics, the state functions depend separately on orthogonal directions and can be written as a sum over the individual contributions. Hence it is sufficient

to analyze the state functions for the confined direction only, as the contributions from the other directions are trivial. For a simpler notation, we hereafter replace L_1 by L.

The confined region can be represented by a hard-walled potential well. The eigenfunctions and eigenenergies for spinless particles are obtained from the Schrödinger equation, as $\psi_k(x) = \sqrt{2/L}\,\sin \pi k\tilde{x}$ and $\varepsilon_k = \pi^2\hbar^2k^2/2mL^2$, $k = 1, 2, 3, \ldots$, respectively. Here, $\tilde{x} = x/L$ is the dimensionless coordinate. Hereby, the discrete de Broglie wavelengths corresponding to the eigenfunctions satisfying the boundary conditions are $\lambda_k = 2L/k$, which corresponds to the momentum eigenvalues, but not λ_{th}.

We introduce the normalized eigenenergies $\tilde{\varepsilon} = \varepsilon/k_BT = (\alpha k)^2$, where $\alpha = \sqrt{T_0/T} = 1/\sqrt{\tilde{T}}$ with the temperature $T_0 = \varepsilon_1/k_B$ corresponding to the ground state energy $\varepsilon_1 = \pi^2\hbar^2/2mL^2$.

While the global quantities depend only on the energy spectrum $\{\varepsilon_k\}$, local quantities also strongly depend on the quantum probability distribution $|\psi_k(x)|^2$. In this section, the quantities are defined in their dimensionless forms for the numerical examinations. The local density is given by

$$\tilde{n} = \frac{n}{n_{Gl}} = \frac{\sum_{k=1}^{\infty} e^{-\frac{\varepsilon_k}{k_BT}}|\psi_k(x)|^2}{\frac{1}{L}\sum_{k=1}^{\infty} e^{-\frac{\varepsilon_k}{k_BT}}} = \frac{2\sum_{k=1}^{\infty} e^{-(\alpha k)^2}\sin^2(\pi k\tilde{x})}{\sum_{k=1}^{\infty} e^{-(\alpha k)^2}} \tag{8}$$

and shows that n is a function of the temperature, although the global one n_{Gl} is not. Hence, in the quantum limit, γ_L does not vanish and, by using Eq. (8), it is determined in dimensionless form as

$$\tilde{\gamma}_L = -\frac{T}{n_{Gl}}\left(\frac{\partial n}{\partial T}\right)_L = -T\left(\frac{\partial \tilde{n}}{\partial T}\right)_L = (\hat{U} - \hat{u})\tilde{n}, \tag{9}$$

where

$$\hat{U} = \frac{U}{Nk_BT} = \frac{\sum_{k=1}^{\infty}(\alpha k)^2 e^{-(\alpha k)^2}}{\sum_{k=1}^{\infty} e^{-(\alpha k)^2}}, \tag{10a}$$

$$\hat{u}(\tilde{x}) = \frac{u}{nk_BT} = \frac{\sum_{k=1}^{\infty}(\alpha k)^2 e^{-(\alpha k)^2}\sin^2(\pi k\tilde{x})}{\sum_{k=1}^{\infty} e^{-(\alpha k)^2}\sin^2(\pi k\tilde{x})}. \tag{10b}$$

The last equality in Eq. (9) indicates that, in the case of Maxwell statistics, γ_L is related with the deviations of global energy $\hat{U}$ from its local value $\hat{u}$.

γ_L plays a crucial role in nanoscale systems and the terms containing γ_L in Eqs. (4a)–(7b) represent the quantum migration corrections. If we had considered a position-dependent confinement potential or a particle-wall interaction potential (as in a classical real gas), this would also result in a temperature-dependent density profile, leading to a nonzero γ_L. On the other hand, here we consider a noninteracting gas and a position-independent potential within the domain and we still get a nonzero γ_L just because of the wave nature of the particles, showing that what we are considering here is a purely quantum term.

In the classical case ($\hbar \to 0$), $|\psi_k(x)|^2 \to 1/L$, and all local quantities go to their classical counterparts. In such a case, $\alpha \to 0$, $\tilde{n} \to 1$, $\tilde{\gamma}_L \to 0$, $\hat{u}$, and $\hat{U} \to 1/2$. Note that the infinite summations in Eqs. (8), (10a), and (10b) can either be numerically calculated or analytically represented by Jacobi (elliptic) theta function $\upsilon_3(0, e^{-\alpha^2})$ and its derivatives with respect to α^2.

The dimensionless forms of the local and global heat capacities can be defined as $\tilde{c}_L = c_L/(n_{Gl}k_B)$ and C_L/Nk_B, respectively, by considering the temperature independent (constant) quantities n_{Gl} and N.

The spatial and temperature variations of density, thermal expansion coefficient, energy, and temperature derivative of local energy, $\tilde{c}_L^{u,0}$, are displayed in Figs. 1(b)–1(f). In the high temperature limit, all the quantities approach their classical values in the expanding homogeneous central region, including $c_L^{u,0} \to 1/2$. By contrast, at low temperatures, due to the strong confinement the density becomes highly inhomogeneous and particles accumulate in the central region, Fig. 1(b). This results in regions of excess, $\tilde{n} > 1$ (between the black curves), and depletion, $\tilde{n} < 1$ (between the boundaries and the black curves), of density.

The temperature dependency of density leads to nonzero isometric thermal expansion of density in general, $\tilde{\gamma}_L \neq 0$. The excess density at the domain center decreases with rising temperature and implies that $\tilde{\gamma}_L > 0$ (between the white curves), while the density increment near the boundaries shows thermal contraction, $\tilde{\gamma}_L < 0$ (between the boundaries and the white curves); see Figs. 1(b) and 1(c). $\tilde{\gamma}_L$ is maximal at the domain center, $\tilde{\gamma}_L^{\max} = 0.43$ for $\tilde{T} = 1.8$. The thermally expansive region is bounded to $1/3 < \tilde{x} < 2/3$ for temperatures $\tilde{T} < 1$. Near the boundaries, $\tilde{\gamma}_L \leqslant 0$ and its minimum is pushed towards the domain boundaries as temperature increases and its value remains almost constant as $\tilde{\gamma}_L^{\min} = -0.37$. The nonzero value of $\tilde{\gamma}_L$ is a purely quantum effect and it is the physical mechanism behind the *temperature-induced quantum migration* which influences the local energy transport within the domain. The internal energy per particle, see Fig. 1(d), assumes nearly its classical value 1/2 at the central region for high temperatures and approaches 3/2 at the boundaries [56]. This explicitly shows the accumulation of thermal energy per particle near boundaries. At low temperatures, the thermal contribution vanishes and the energy per particle becomes uniform, Fig. 1(d), equaling the ground state energy, $\alpha^2 = 1/\tilde{T}$. The local energy $\tilde{u} = \hat{u}\tilde{n}$, on the other hand, vanishes on the boundary since $\tilde{n}$ does. Nevertheless, except for the low temperatures, the local energy is maximal near the boundaries—the green region (close to the inner side of dotted black curve) in Fig. 1(e). For $\tilde{T} \ll 1$, the local energy maximum shifts to the center of the domain, by approving $\tilde{u} \to 2\,\sin^2(\pi\tilde{x})/\tilde{T}$.

The temperature derivative of local energy, $\tilde{c}_L^{u,0}$, is plotted in Fig. 1(f). At low temperature, an interesting behavior appears and it takes negative values, $\tilde{c}_L^{u,0} < 0$, around the domain center, encircled by white curve, assuming its minimum -0.23 at $\tilde{T} = 0.98$. Hence the existence of a negative region confirms that $\tilde{c}_L^{u,0}$ cannot by itself represent the local heat capacity.

In Fig. 2, we plot the local (a) conductive, $\tilde{c}_L^{\text{cnd}}$, (b) quantum migration, $\tilde{c}_L^{\text{qmh}}$, and (c) total, $\tilde{c}_L^{\text{tot}}$, heat capacities by considering the following dimensionless forms of Eqs. (2b), (3b), (6),

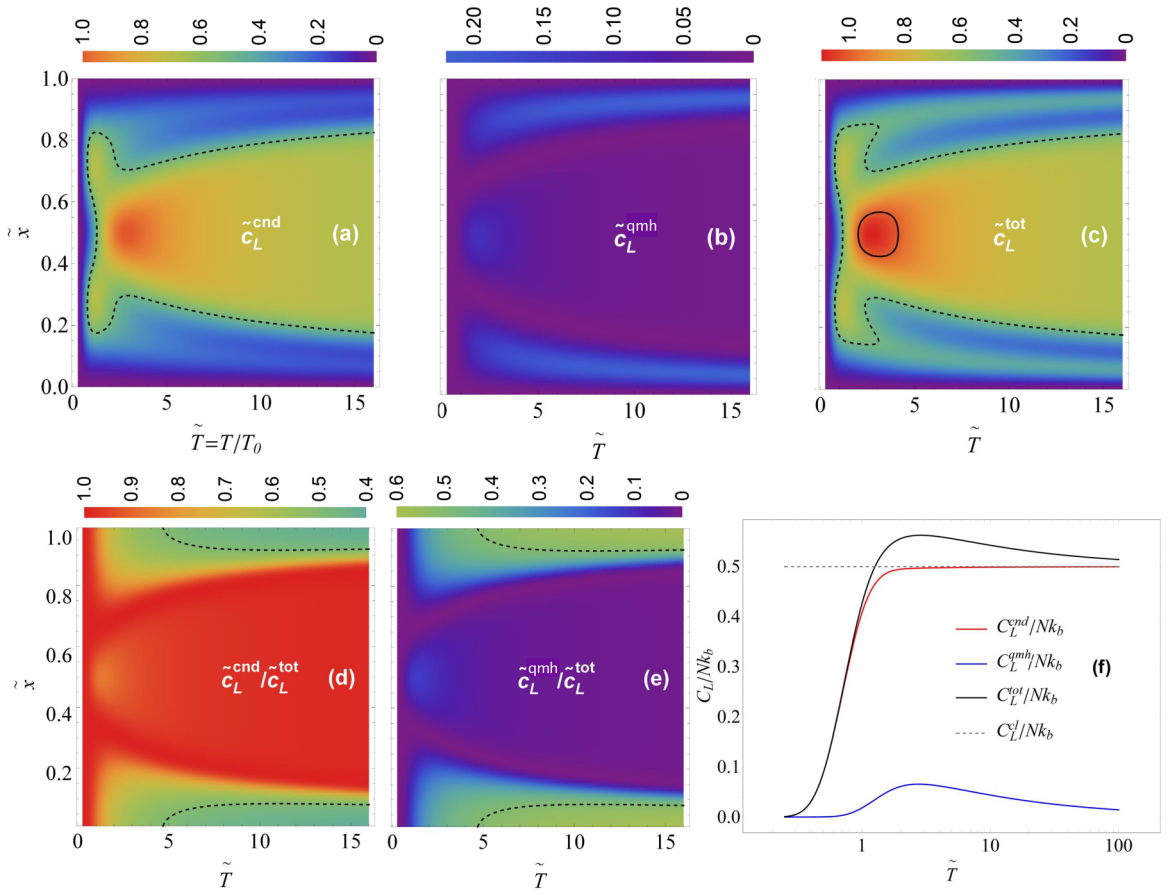

FIG. 2. Variations of local and global constant-size heat capacities and their components. The dotted black curves represent the value of $1/2$, while the black curve in (c) stands for 1.

and (7b), respectively,

$$\tilde{c}_L^{\mathrm{cnd}} = \tilde{c}_L^{u,0} + \hat{\omega}\tilde{\gamma}_L = \tilde{c}_L^{u,0} + (\hat{u}+1)\tilde{\gamma}_L, \tag{11}$$

$$\tilde{c}_L^{\mathrm{qmh}} = (\hat{\Omega}-\hat{\omega})\tilde{\gamma}_L = (\hat{U}-\hat{u})\tilde{\gamma}_L, \tag{12}$$

$$\tilde{c}_L^{\mathrm{tot}} = \tilde{c}_L^{u,0} + \tilde{c}_L^{\mathrm{u,QC}} = \tilde{c}_L^{u,0} + (\hat{U}+1)\tilde{\gamma}_L, \tag{13}$$

where $\hat{\omega} = \omega/(nk_BT)$ and $\hat{\Omega} = \Omega/(Nk_BT)$. Note that for non-interacting Maxwell gas, $\hat{\omega} = \hat{u}+1$ and $\hat{\Omega} = \hat{U}+1$ as $\varphi = -nk_BT$ and $\Phi = -Nk_BT$, respectively.

Figure 2 shows that total heat capacity and its conductive and QMH components are all positive throughout the domain for all temperatures. Moreover, for low temperatures, both the conductive and total heat capacities are maximal at the center, while the QMH capacity has a weaker local maximum at the center and stronger global maxima regions (lighter colors) near boundaries.

The local heat capacity has a massive overshoot, $\tilde{c}_L^{\max} \approx 1.1$, at the center for $\tilde{T} = 2.73$; see the region encircled by the black curve in Fig. 2(c). This is more than twice the classical value $1/2$ and signifies the importance of quantum migration for the local heat capacity. The results in Figs. 2(d) and 2(e), furthermore, indicate that the conductive contribution is widely dominant (almost 100%) in the central region, while the QMH is dominating near the boundary regions by approaching $2/3$, for $\tilde{T} > 1$. The quantum migration leads to an accumulation of energy near the boundaries and is responsible for building up the thermal part of confinement energy.

The total (global) heat capacity, Fig. 2(f) (black, at the top), overshoots, $C_L^{\mathrm{tot}}/Nk_B \to 0.5625 > 1/2$, at $\tilde{T} = 2.86$, in excellent agreement with previous results [2,31,37]. Furthermore, while the conductive contribution (red, in the middle) is always less than the classical limit $1/2$, the contribution of QMH (blue, at the bottom) increases up to a critical temperature, $\tilde{T} = 2.86$, and diminishes for $\tilde{T} > 2.86$, showing that TIQM and accordingly QMH provides the overshoot of global heat capacity.

Figure 3(a) shows the variations of $\tilde{c}_L^{u,\mathrm{QC}}$. Due to QMH, the local heat capacity increases in the central region and decreases near the boundaries, corresponding to the fact that heat is absorbed at the center and subsequently deposited near the boundaries.

In particular, heat is absorbed within the region between the white curves in Fig. 3(a), while rejected outside this zone. Thus heat energy is carried from the central region towards the near boundaries through QMH driven by TIQM. A comparison between Figs. 2(c) and 3(a) shows that $\tilde{c}_L^{\mathrm{QC}}$ constitutes more than 50% of $\tilde{c}_L^{\mathrm{tot}}$ at the center and near the boundaries. For increasing temperatures, the heat absorption region grows wider and becomes less significant. By contrast, the heat deposition region is pushed closer towards the boundaries and maintains its crucial contribution.

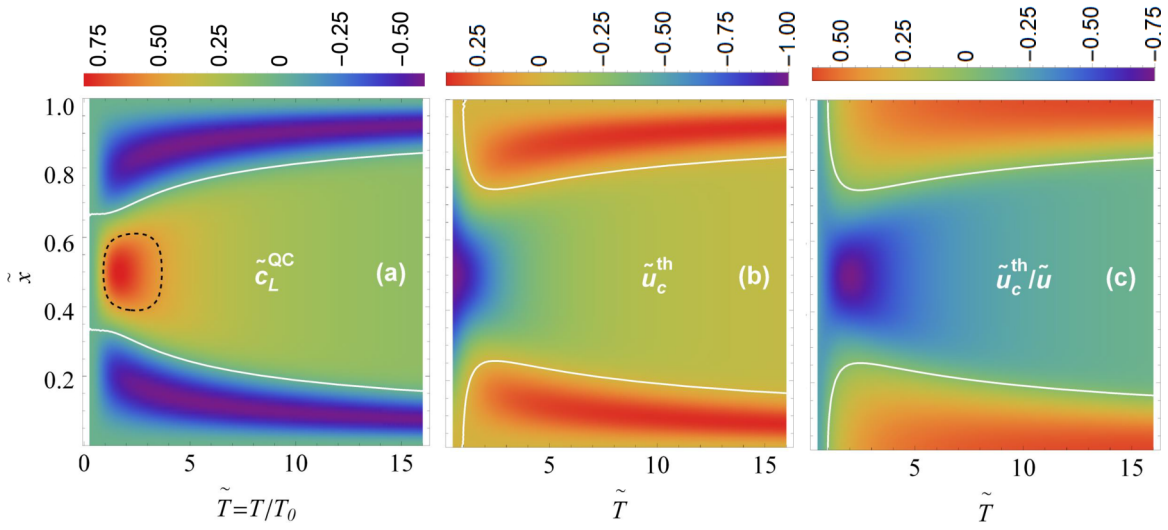

FIG. 3. Variations of total correction of QC for local heat capacity (a), thermal part of confinement energy (b), and the percentage of the thermal part of confinement energy in total energy (c). The white curve represents the zero crossings, while the dotted black curves stand for 1/2.

The local energy per particle, $\hat{u}$, is a summation of the classical thermal energy 1/2 (contributions from the continuous excited states), the ground state energy α^2, and thermal confinement energy, also known as excess thermal energy, $\hat{u}_c^{\rm th}$ (originating from the discreteness of excited states), defined by

$$\tilde{u}_c^{\rm th} = \frac{u_c^{\rm th}}{n_{Gl} k_B T} = \hat{u}_c^{\rm th} \tilde{n} = \left(\hat{u} - \frac{1}{2} - \alpha^2\right)\tilde{n}. \tag{14}$$

The excess heat capacity emerges from $\tilde{u}_c^{\rm th}$ as the ground state does not contribute to the heat capacity. Similarly, the global excess heat capacity, Fig. 2(f) blue (at the top), results from the QMH contribution. Therefore, the emerging mechanism of $\tilde{u}_c^{\rm th}$ is related to TIQM.

Figure 3(b) shows that $\tilde{u}_c^{\rm th}$ accumulates near boundaries, reminiscent of the QMH contribution to the local heat capacity; cf. Fig. 2(b). In addition, the ratio $\tilde{u}_c^{\rm th}/\tilde{u}$ is as large as 66% near the boundaries, Fig. 3(c), correlating well with the QMH contribution to the local heat capacity, see Fig. 2(e), unequivocally showing that TIQM is the mechanism of the thermal confinement energy in finite systems.

IV. ENERGY FLUCTUATIONS IN EQUILIBRIUM AT THE GLOBAL AND LOCAL SCALES

In macroscopic thermodynamics, heat capacity and energy fluctuations are linearly related in equilibrium. Also, the relative standard deviation of energy fluctuations is inversely proportional to the square root of the total number of particles. Consequently, a large number of particles minimizes the energy fluctuations. In nanoscale systems, however, given the relatively small number of particles and the influence of confinement, it is necessary to verify that the energy fluctuations on both global and local scales are negligible and to check the validity of their relations with the corresponding heat capacities. A comprehensive overview of the thermodynamic theory of equilibrium fluctuations can be found in Ref. [57]. As confined systems are inherently nonextensive, particularly the Ref. [58] can be instrumental in elucidating the general nature of thermodynamic stability criteria and fluctuation theory in nonextensive thermodynamics. In this section, we derive and discuss the global and local energy fluctuations and their relations with the relevant heat capacities.

For the considered domain in Fig. 1(a), the global and local ensemble averages of the moments of energy are given in MB statistics for the confined direction respectively as

$$\langle \varepsilon^d \rangle_{Gl} = \frac{\sum_{k=1}^{\infty} \varepsilon_k^d e^{-\frac{\varepsilon_k}{k_B T}}}{\sum_{k=1}^{\infty} e^{-\frac{\varepsilon_k}{k_B T}}}, \tag{15}$$

$$\langle \varepsilon^d \rangle_{l} = \frac{\sum_{k=1}^{\infty} \varepsilon_k^d e^{-\frac{\varepsilon_k}{k_B T}} \sin^2(\pi k \tilde{x})}{\sum_{k=1}^{\infty} e^{-\frac{\varepsilon_k}{k_B T}} \sin^2(\pi k \tilde{x})}, \tag{16}$$

where d is the moment order of energy. In terms of ensemble averages, global energy is $U = N\langle\varepsilon\rangle_{Gl} = Nk_BT\langle\tilde{\varepsilon}\rangle_{Gl} = Nk_BT\hat{U}$ and hence the global heat capacity is

$$C_L = Nk_B\hat{C}_L = \frac{\mathrm{Var}(U)}{k_B T^2}, \tag{17}$$

where $\mathrm{Var}(U) = N(k_BT)^2[\langle\tilde{\varepsilon}^2\rangle_{Gl} - \langle\tilde{\varepsilon}\rangle_{Gl}^2]$ is the total variance of the global energy. Therefore, the relative standard deviation of global energy is

$$D_R(U) = \frac{\sqrt{\mathrm{Var}(U)}}{U} = \frac{1}{\sqrt{N}} \frac{\sqrt{\hat{C}_L}}{\hat{U}}. \tag{18}$$

For high and low temperature limits, $\tilde{T} \gg 1$ and $\tilde{T} \ll 1$, $\sqrt{\hat{C}_L}/\hat{U}$ goes to $\sqrt{2}$ and 0, respectively. Therefore, as long as the value of N is sufficiently large, the global energy fluctuations will always be negligible. This condition can be readily satisfied by selecting L_2 and L_3 to be long enough, provided that the condition of MB statistics, $\lambda_{\rm th} \ll \sqrt{(L_2L_3)/N}$, is still met. Consequently, even for finite systems, the global energy variance is linearly proportional to the heat capacity, Eq. (17),

and the magnitude of the relative fluctuations is inversely proportional to $\sqrt{N}$, Eq. (18).

Using Eqs. (9), (13), (15), and (16), local heat capacity can be written in terms of local and global ensemble averages as

$$c_L = nk_B[\langle\tilde{\varepsilon}^2\rangle_l - 2\langle\tilde{\varepsilon}\rangle_l\langle\tilde{\varepsilon}\rangle_{Gl} + \langle\tilde{\varepsilon}\rangle_{Gl}^2 + \langle\tilde{\varepsilon}\rangle_{Gl} - \langle\tilde{\varepsilon}\rangle_l] = nk_B\hat{c}_L \neq \frac{\mathrm{Var}(u)}{k_BT^2}, \tag{19}$$

where $\mathrm{Var}(u) = n(k_BT)^2[\langle\tilde{\varepsilon}^2\rangle_l - \langle\tilde{\varepsilon}\rangle_l^2]$ is the total variance of the local energy. It seems that the linear relation between the energy variance and heat capacity is broken at the local scale. The relative standard deviation of local energy is written by considering the local energy in the form of $u = nk_BT\hat{u}$, as

$$D_R(u) = \frac{\sqrt{\mathrm{Var}(u)}}{u} = \frac{1}{\sqrt{n}}\frac{\sqrt{\langle\tilde{\varepsilon}^2\rangle_l - \langle\tilde{\varepsilon}\rangle_l^2}}{\hat{u}}. \tag{20}$$

Equation (20) shows that $D_R(u)$ remains negligible as long as $n = n_{Gl}\tilde{n}$ is sufficiently large. Since $n_{Gl} = N/L$ consists of a large total number of particles N in a small size L, n takes very high values almost everywhere across the domain, except the regions very close to the boundaries, where $\tilde{n} \ll 1$. The higher the value of n_{Gl}, the higher the value of n and the closer to the boundary the region where fluctuations are negligible. In the macroscopic limit, $\langle\rangle_l \to \langle\rangle_{Gl}$ and $\tilde{n} \to 1$, and the following conventional relations are recovered also for local quantities:

$$c_L \to n_{Gl}k_B\left[\langle\tilde{\varepsilon}^2\rangle_{Gl} - \langle\tilde{\varepsilon}\rangle_{Gl}^2\right] = n_{Gl}k_B\tilde{c}_L, \tag{21}$$

$$\mathrm{Var}(u) \to n_{Gl}(k_BT)^2\tilde{c}_L. \tag{22}$$

Equations (18) and (20) manifest that, during a quasistatic and isometric heat exchange process, both global and local fluctuations are at negligible level in the context of the presented problem, as long as $N \gg 1$ and $\lambda_{\mathrm{th}} \ll \sqrt{(L_2L_3)/N}$, which is met by the macroscopic values of L_2 and L_3. The negligible nature of fluctuations remains consistent even if there is only one domain size at the macroscopic level, provided that the system involves a large number of particles.

V. CONCLUSION

To uncover the TIQM phenomenon, we consider quasiequilibrium changes in local density and other state functions in response to infinitesimal temperature change. The results represent a reference case based on Maxwell-Boltzmann statistics and the consideration of Fermi-Dirac and Bose-Einstein statistics extends the study to investigate the effects of degeneracy, thus allowing a wider range of materials to be considered for possible experiments. For the confinement domain considered here, weaker and stronger quantum migration processes and corresponding contributions to the local heat capacity are expected for Fermi and Bose gases, respectively. A further extension of the study is the construction of transport models that include the nonequilibrium and transient states of the TIQM process.

In a real gas, particle-wall interactions disrupt the uniformity of density in a thin layer near the domain boundaries and induce classical size effects that give rise to surface, edge, and corner energies. Temperature variation alters these size effects by modifying the nonuniform density profile and causes a similar type of net particle motion. However, due to the short-range nature of particle-wall interactions, this particle motion only occurs within a thin layer close to the walls. Here we show that even in a noninteracting gas and in the absence of gravitational or other potential fields, quantum migration is extensively induced throughout the whole domain because of the wave nature of the particles.

Therefore, quantum migration is a fundamental and crucial process in nanoscale systems, making an indispensable contribution to the local heat capacity. It induces a massive overshoot in local capacity and explains the excess global heat capacity reported previously [2,37–41]. It leads to both qualitatively and quantitatively correct results for the local heat capacity. Even in a ballistic regime where viscosity loses its meaning, quantum migration continues to exist. Moreover, the thermal part of the confinement energy, which is the origin of many unusual properties of confined systems, is built up by the TIQM process.

Experimental observation of the massive local heat capacity will unequivocally reveal the importance of the macroscopic quantum phenomenon introduced here. Therefore, one of the reasonable ways to verify the contribution of TIQM, and accordingly QMH, is to measure the overshoot in local heat capacity appearing at the center of the domain at low temperatures, $\tilde{T} < 5$. Scanning thermal microscopy can be a useful tool for this purpose. Doped silicon thermoresistive probes offer relatively high spatial (10 nm) and temperature (7 mK) resolutions [59]. Dynamic (transient) heat transport measurements with such a device may provide information about the local volumetric heat capacity with high spatial resolution [60]. As the de Broglie wavelength of atomic particles is too small, one of the reasonable candidates can be a low-doped monocrystalline n-type GaAs semiconductor due to the low effective mass ($m^* = 0.067$) of the conduction electrons [61]. Low doping allows us to use Maxwell-Boltzmann statistics and also minimizes the effect of impurity scatterings while a monocrystalline structure eliminates the effect of defects. A quantum well structure made of this material can serve as a sample for experimental measurements of the local heat capacity maximum. A simple calculation considering $\tilde{T} \approx 2.73$ and $m^* = 0.067$ shows that the necessary thickness of such a sample should be roughly in between 240 nm and 40 nm to observe the local heat capacity maximum at 3 K and 100 K temperatures, respectively. Such thicknesses allow the possibility of using scanning thermal microscopy. Extending the results to include quantum statistics will provide even greater flexibility for the experimental studies.

[1] E. Roduner, *Nanoscopic Materials, Size-Dependent Phenomena* (RSC Publishing, Cambridge, UK, 2006).

[2] F. Binder, L. Correa, C. Gogolin, J. Anders, and G. Adesso, *Thermodynamics in the Quantum Regime: Fundamental Aspects*

and New Directions, Fundamental Theories of Physics (Springer, Berlin, 2018).
[3] M. Mondal and K. Ghatak, Effect of size quantization on the electronic heat capacity in ultrathin films of semiconductors, Phys. Status Solidi B **120**, K63 (1983).
[4] Y. Volokitin, J. Sinzig, L. J. de Jongh, G. Schmid, M. N. Vargaftik, and I. I. Moiseevi, Quantum-size effects in the thermodynamic properties of metallic nanoparticles, Nature (London) **384**, 621 (1996).
[5] M. I. Molina, Ideal gas in a finite container, Am. J. Phys. **64**, 503 (1996).
[6] G. Gutierrez and J. M. Yanez, Can an ideal gas feel the shape of its container? Am. J. Phys. **65**, 739 (1997).
[7] R. K. Pathria, An ideal quantum gas in a finite-sized container, Am. J. Phys. **66**, 1080 (1998).
[8] W. S. Dai and M. Xie, Quantum statistics of ideal gases in confined space, Phys. Lett. A **311**, 340 (2003).
[9] A. Sisman and I. Muller, The Casimir-like size effects in ideal gases, Phys. Lett. A **320**, 360 (2004).
[10] A. Sisman, Surface dependency in thermodynamics of ideal gases, J. Phys. A: Math. Gen. **37**, 11353 (2004).
[11] W. S. Dai and M. Xie, Geometry effects in confined space, Phys. Rev. E **70**, 016103 (2004).
[12] W. S. Dai and M. Xie, Hard-sphere gases as ideal gases with multi-core boundaries: An approach to two-and three-dimensional interacting gases, Europhys. Lett. **72**, 887 (2005).
[13] H. Pang, W. S. Dai, and M. Xie, The difference of boundary effects between bose and Fermi systems, J. Phys. A: Math. Gen. **39**, 2563 (2006).
[14] A. Sisman, Z. F. Ozturk, and C. Firat, Quantum boundary layer: A non-uniform density distribution of an ideal gas in thermodynamic equilibrium, Phys. Lett. A **362**, 16 (2007).
[15] W. S. Dai and M. Xie, Interacting quantum gases in confined spaces: Two-and three-dimensional equation of state, J. Math. Phys. **48**, 123302 (2007).
[16] C. Firat and A. Sisman, Universality of quantum boundary layer for a maxwellian gas, Phys. Scr. **79**, 065002 (2009).
[17] C. Firat, A. Sisman, and Z. F. Ozturk, Thermodynamics of gases in nano-cavities, Energy **35**, 814 (2010).
[18] H. Pang, W. S. Dai, and M. Xie, The pressure exerted by a confined ideal gas, J. Phys. A: Math. Theor. **44**, 365001 (2011).
[19] C. Firat and A. Sisman, Quantum forces of a gas confined in nano structures, Phys. Scr. **87**, 045008 (2013).
[20] A. Aydin and A. Sisman, Discrete nature of thermodynamics in confined Fermi gases, Phys. Lett. A **378**, 2001 (2014).
[21] S. Kjelstrup, S. K. Schnell, T. J. H. Vlugt, J. M. Simon, A. Bardow, D. Bedeaux, and T. Trinh, Bridging scales with thermodynamics: from nano to macro, Adv. Nat. Sci: Nanosci. Nanotechnol. **5**, 023002 (2014).
[22] A. Aydin and A. Sisman, Dimensional transitions in thermodynamic properties of ideal maxwell-boltzmann gases, Phys. Scr. **90**, 045208 (2015).
[23] A. Aydin and A. Sisman, Discrete density of states, Phys. Lett. A **380**, 1236 (2016).
[24] S. Karabetoglu and A. Sisman, Thermosize potentials in semiconductors, Phys. Lett. A **381**, 2704 (2017).
[25] A. Aydin and A. Sisman, Quantum oscillations in confined and degenerate Fermi gases. I. Half-vicinity model, Phys. Lett. A **382**, 1807 (2018).
[26] A. Aydin and A. Sisman, Quantum oscillations in confined and degenerate Fermi gases. II. The phase diagram and applications of half-vicinity model, Phys. Lett. A **382**, 1813 (2018).
[27] A. Aydin and A. Sisman, Quantum shape effects and novel thermodynamic behaviors at nanoscale, Phys. Lett. A **383**, 655 (2019).
[28] A. Aydin, Quantum shape effects, Ph.D. thesis, Istanbul Technical University, 2020.
[29] A. Aydin, A. Sisman, and R. Kosloff, Landauers principle in a quantum szilard engine without maxwells demon, Entropy **22**, 294 (2020).
[30] A. Sisman and J. Fransson, Fractional integral representation in statistical thermodynamics of confined systems, Phys. Rev. E **104**, 054110 (2021).
[31] H. O. Batael, E. D. Filho, J. Chahine, and J. F. Silva, Effects of quantum confinement on thermodynamic properties, Eur. Phys. J. D **75**, 247 (2021).
[32] A. Aydin, J. Fransson, and A. Sisman, Quantum shape oscillations in the thermodynamic properties of confined electrons in coreshell nanostructures, J. Phys.: Condens. Matter **34**, 025301 (2022).
[33] A. Aydin and A. Sisman, Origin of the quantum shape effect, Phys. Rev. E **108**, 024105 (2023).
[34] A. Aydin, J. Fransson, and A. Sisman, Thermosize voltage induced in a ballistic graphene nanoribbon junction, J. Appl. Phys. **126**, 104302 (2019).
[35] A. Sisman, A. Aydin, and J. Fransson, Thermoshape effect for energy harvesting with nanostructures, J. Phys. D: Appl. Phys. **53**, 375501 (2020).
[36] A. Aydin, A. Sisman, J. Fransson, A. Black-Schaffer, and P. Dutta, Thermodefect voltage in graphene nanoribbon junctions, J. Phys.: Condens. Matter **34**, 195304 (2022).
[37] H. B. Rosenstock, Specific heat of a particle in a box, Am. J. Phys. **30**, 38 (1962).
[38] L. Gold, On the wave mechanics of gases, Nuovo Cimento **32**, 1622 (1964).
[39] F. E. Cummings, The particle in a box is not simple, Am. J. Phys. **45**, 158 (1977).
[40] C. A. Pizarro, C. A. Condat, P. W. Lamberti, and D. Prato, Specific heat revisited, Am. J. Phys. **64**, 736 (1996).
[41] V. Granados and N. Aquino, Comment on "specific heat revisited," by C. A. Pizarro, C. A. Condat, P. W. Lamberti, and D. P. Prato, Am. J. Phys. **67**, 450 (1999).
[42] P. Serra, M. A. Carignano, F. H. Alharbi, and S. Kais, Quantum confinement and negative heat capacity, Europhys. Lett. **104**, 16004 (2013).
[43] M. A. Carignano and I. Gladich, Negative heat capacity of small systems in the microcanonical ensemble, Am. J. Phys. **90**, 63001 (2010).
[44] H. Hasegawa, Specific heat anomalies of small quantum systems subjected to finite baths, J. Math. Phys. **52**, 123301 (2011).
[45] J. Rao, Q. Liu, T. Liu, and L. Li, Negative specific heat, phase transition and particles spilling from a potential well, Ann. Phys. (NY) **323**, 1415 (2008).
[46] M. Schmidt, R. Kusche, T. Hippler, J. Donges, W. Kronmuller, B. vonIssendorff, and H. Haberland, Negative heat capacity for a cluster of 147 sodium atoms, Phys. Rev. Lett. **86**, 1191 (2001).
[47] R. S. Berry, Remarks on negative heat capacities of clusters, Isr. J. Chem. **44**, 211 (2004).

[48] D. Lynden-Bell, Negative specific heat in astronomy, physics and chemistry, Physica A **263**, 293 (1999).

[49] D. Lynden-Bell and R. Lynden-Bell, On the negative specific heat paradox, Mon. Not. R. Astron. Soc. **181**, 405 (1977).

[50] H. A. Posch and W. Thirring, Stellar stability by thermodynamic instability, Phys. Rev. Lett. **95**, 251101 (2005).

[51] L. Velazquez and S. Curilef, On the thermodynamic stability of macrostates with negative heat capacities, J. Stat. Mech. (2009) P03027.

[52] R. T. Waechter, On hearing the shape of a drum: an extension to higher dimensions, Proc. Cambri. Philos. Soc. **72**, 439 (1972).

[53] W. Arendt, R. Nittka, W. Peter, and F. Steiner, in *Mathematical Analysis of Evolution, Information, and Complexity*, edited by W. Arendt and W. P. Schleich (Wiley-VCH, New York, 2009).

[54] J. T. Knuiman, P. Borneveld, and N. Besseling, On the relation between the fundamental equation of thermodynamics and the energy balance equation in the context of closed and open systems, J. Chem. Educ. **89**, 968 (2012).

[55] C. Goupil, W. Seifert, K. Zabrocki, E. Müller, and G. J. Snyder, Thermodynamics of thermoelectric phenomena and applications, Entropy **13**, 1481 (2011).

[56] For the boundary regions and high-temperature conditions, Taylor expansion can be used for $\sin^2 x$ functions in Eq. (10b) and, also, an integral approach can be applied for the summations to obtain the value of 3/2 for $\hat{u}$.

[57] Y. Mishin, Thermodynamic theory of equilibrium fluctuations, Ann. Phys. (NY) **363**, 48 (2015).

[58] Y. Zheng, J. Du, and F. Liang, Thermodynamic stability criterion and fluctuation theory in nonextensive thermodynamics, Continuum Mech. Thermodyn. **30**, 629 (2018).

[59] Y. Zhang, W. Zhu, F. Hui, M. Lanza, T. Borca-Tasciuc, and M. M. Rojo, A review on principles and applications of scanning thermal microscopy (SThM), Adv. Funct. Mater. **30**, 1900892 (2020).

[60] T. Haeger, M. Wilmes, R. Heiderhoff, and T. Riedl, Simultaneous mapping of thermal conductivity, thermal diffusivity, and volumetric heat capacity of halide perovskite thin films: A novel nanoscopic thermal measurement technique, J. Phys. Chem. Lett. **10**, 3019 (2019).

[61] C. W. J. Beenakker and H. van Houten, Quantum transport in semiconductor nanostructures, Solid State Phys. **44**, 1 (1991).